

High speed BLDC motor for grid tied PV based EV system using hybrid PSO-spotted hyena optimized PI controller

S. Prakash, K. Boopathy

Department of Electrical and Electronics Engineering, Aarupadai Veedu Institute of Technology,
Vinayaka Missions Research Foundation, Chennai, India

Article Info

Article history:

Received Aug 26, 2023

Revised Mar 23, 2024

Accepted Apr 29, 2024

Keywords:

BLDC motor

Electric vehicle

High gain improved Luo converter

Photovoltaic

PS-SHO optimized PI controller

ABSTRACT

The rapid adoption of electric vehicle (EV) motors has recently raised numerous issues including high expensive, complex maintenance, and resonance problems. Some of the most effective and most thoroughly investigated EV motors are 3 ϕ induction motors and DC motors. Brushless DC (BLDC) motors for EVs are a more advanced version of the solution used in developing nations. Rising time, steady state, transient, overshoot, settling time and other characteristics of the EV based BLDC motor are difficult to control. A loss of control leads to system instability and reduces the components' lifespan. Thereby, in this work, a grid incorporated PV fed EV based BLDC motor is proposed using DC-DC converter along with hybrid optimized PI controller. An innovative high gain Luo converter has been developed with the goal to deal with the fluctuating behavior of PV systems and it provides the impressive advantages of a high conversion range, reduced voltage stress and outstanding efficiency. To considerably improve the performance of the suggested converter, the reliable hybrid particle swarm-spotted hyena optimized (PS-SHO) proportional integral (PI) controller is invented for controlling the BLDC motor's speed. The grid supplies electricity to the BLDC motor when the PV-based power source isn't accessible. The simulation used to determine the efficacy of the proposed BLDC motor system in MATLAB has confirmed that the methodology provides increased efficacy with a highest efficiency of 97.3% and a lower total harmonic distortion (THD) of 2.02%.

This is an open access article under the [CC BY-SA](https://creativecommons.org/licenses/by-sa/4.0/) license.



Corresponding Author:

S. Prakash

Department of Electrical and Electronics Engineering, Aarupadai Veedu Institute of Technology,

Vinayaka Missions Research Foundation

Chennai, Tamil Nadu 600010, India

Email: prakash.yours@gmail.com

1. INTRODUCTION

The decreasing supply of fossil fuels and rising carbon emissions are driving consumers to switch the energy towards renewable sources. Photovoltaic (PV) production is quickly overtaking traditional sources as the most suitable choice for a variety of appliances [1]. Considering this, the EV has drawn considerable devotion in the past few years as a vital PV source of energy. In an effort to increase the effectiveness and efficacy of PV-fed EV systems while lowering prices, a large number of research on electric motor drives have been carried out [2], [3]. EVs are essential for the operation of energy systems, batteries, power converters and motor drives. However, the somewhat restricted driving range caused by limitations in present battery technology prevents EVs from being used extensively [4], [5]. Powerful starting torque, quick dynamic response, strong torque ripple and acoustic noise are characteristics of switched reluctance motor

drives that match the requirements for wide application of EVs. A solar panel and a brushless DC (BLDC) motor drive are offered as solutions to these problems. To create a sustainable energy source, a PV panel is attached to the top of the EV [6]. Since the past few years, people have selected the BLDC motors for EV systems, because of its several advantages. Since the BLDC motor has maximum torque ratio and efficiency, minimal electromagnetic interference and low cost of preservation, it is frequently utilised for low and medium power purposes [7], [8]. The BLDC motor is too frequently employed in robotics, medical, aerospace, electric vehicles and servo appliances [9], [10]. These motors require electronic commutators, which depend on rotor location, to perform commutation deploying a voltage source inverter. Because BLDC motors don't require the use of brushes and have excellent speed-torque characteristics, there are fewer eddy current losses and copper losses. The permanent magnet excitation of the BLDC motor prevents excitation losses, which raises the efficiency of the motor to a suitable level [11]. Hence, this paper proposes a PV served BLDC motor for EV applications. The BLDC motor diagram for a PV-fed system is demonstrated in Figure 1.

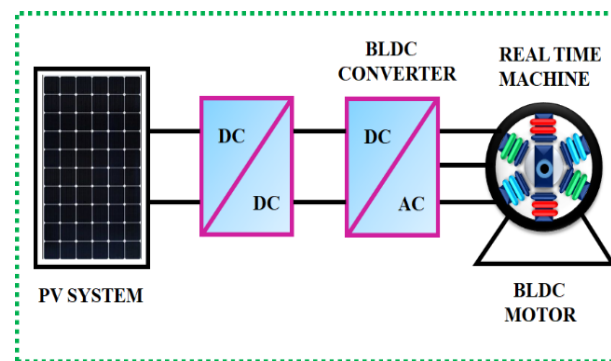


Figure 1. PV fed BLDC motor

Normally, the PV panel has inability to meet the load demand, because of its insufficient dc output voltage. For the purpose of increasing the solar panel output dc voltage, several DC-DC converters are had been proposed. One of the common types of converters frequently utilized in PV applications is the boost [12], [13] converter. Boost converter is utilized to increases voltage input over a broad range. However, because it causes significant voltage stress, it cannot be used in high power applications. Buck-Boost converter's current input fluctuates, while the Cuk converter's input current is non-pulsating. These two converters run at high duty cycles to provide a discontinuous output current and maximize voltage gain [14], [15]. Despite the SEPIC [16] converter's continuous input currents and ability to execute high power applications, the significant number of ripples in input current lowers the thoroughgoing power extraction capabilities of PV over an extensive range. As these converters include built-in voltage boosting characteristics and the capacity to handle high power ratings, Luo converters are in fact the finest option for expanded PV-based EV charging systems. Luo converters [17] have the lowest current ripples and highest output voltage in comparison to other converters. The battery life is negatively impacted by the converter's disadvantage of non-pulsating current at the converter input. Therefore, the high gain improved Luo has been implemented to overwhelmed the restrictions of classical approaches. Utilizing this converter results in lowest voltage stress and highest voltage gain.

For managing the voltage across the DC link in a situation of additional disruptions and unpredictability, a feedback control technique is typically used. Numerous types of controllers have been proposed in [18] to maintain the dc link voltage control, from that proportional integral (PI) controllers are one of the common type controllers. The traditional strategies for adjusting the PI controller's variables include mathematical formula-based approaches that conduct initial assumptions and display arbitrary increase or decrease in error values at any time. Since errors in following approximations are controlled using optimization-based procedures, such methods are highly recommended [19]. The genetic algorithm [20], grey wolf optimization (GWO) and particle swarm optimization (PSO) are three optimization techniques that significantly influence how PI controllers are tuned [21], [22]. However, these algorithms struggle with delayed convergence during the improved search stage and poor local search capability. In regard to these problems, a hybrid particle swarm-spotted hyena optimized (PS-SHO) optimization is implemented to deliver improved control signals to the converter. Thereby, the primary goal of this works is explained as follows:

- A PI controller and a hall sensor control the BLDC motor's speed.

- An improved Luo converter with a high gain has been used to boost the voltage of a PV panel with a considerable reduction in power loss and ripple.
- To use a hybrid PS-SHO optimized PI controller to achieve the suggested converter's maximum conversion efficiency.
- To construct a grid-interactive system that accepts additional solar power during the day and generates electricity at night.
- To maintain the grid current's total harmonic distortion (THD) around 5%.

2. PROPOSED SYSTEM DESCRIPTION

Due to benefits including their straightforward design, great efficacy, exceptional speed control ability, minimal losses and low maintenance requirements EVs are most commonly powered by BLDC motors. Figure 2 illustrates the construction of a PV supplied BLDC motor drive for an EV using a PS-SHO optimized PI controller in this article. The production of power from a PV system is not continuous because it fluctuates with solar irradiation and temperature. PV system resultant voltage is kept as a constant dc output of the right voltage by using a high gain enhanced Luo converter. When compared to traditional PI controller, PS-SHO optimized PI controller offers an excellent possibility for removing the peak overshoot problem with a quick settling time. The converter achieves a stable state with not exceeding the predetermined value by using a properly adjusted PI controller. The 3 ϕ VSI obtains the converter's output dc voltage and transforms it to AC voltage before supplying it to the EV's motor. The basic goal of regulating the motor speed is accomplished with a PI controller. This controller input is error speed produced by analyzing the reference (N_{ref}) and actual (N_{act}) speeds of the motor. The controller output passes into the PWM generator, which produces the appropriate pulses to regulate the switching action of the VSI. Using a 1ϕ VSI, the converter resultant dc voltage is converted to AC voltage and delivered into 1ϕ grid. PI controller is employed to establish grid voltage synchronization. During lack of PV power throughout the night, grid electricity is utilized to power the BLDC motor.

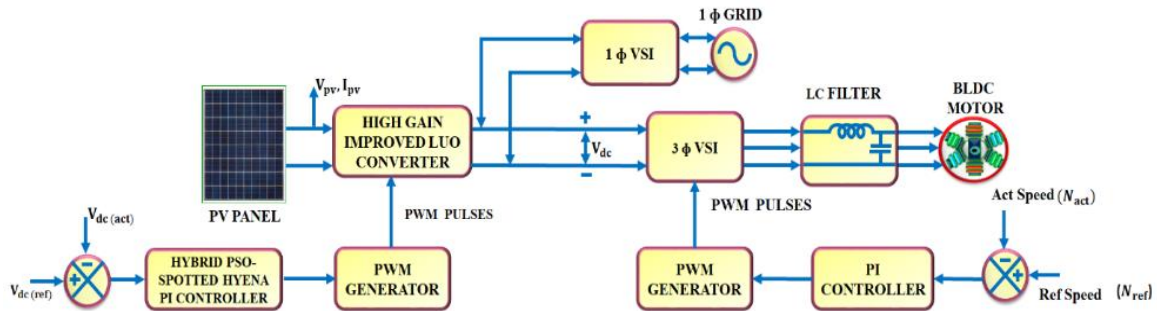


Figure 2. Solar fed BLDC motor using optimized PI controller

3. PROPOSED SYSTEM MODELLING

3.1. PV system modelling

As shown in Figure 3, an analogue circuit of a solar cell consists of a series resistor R_s , a shunt resistor R_{sh} , a current source I_{ph} , and a diode D . Every solar cell that contributes to the solar energy system is depicted by a single diode model. The output current produced by the PV, or I_{PV} , is calculated using (1).

$$I_{PV} = I_{ph} - I_D - I_{Sh} \tag{1}$$

The Shockley equation is used to determine the diode current I_D .

$$I_D = I_o \left[\exp \left(\frac{V_{PV} + R_s I_{PV}}{\alpha V_t N_s} \right) - 1 \right] \tag{2}$$

The current passing via the R_{sh} shunt resistor is.

$$I_{Sh} = \frac{V_{PV} + R_s I_{PV}}{R_{Sh}} \tag{3}$$

Here, the obtain by replacing the values of I_D and I_{sh} in (1).

$$I_{PV} = I_{ph} - I_o \left[\exp\left(\frac{V_{PV} + R_s I_{PV}}{\alpha V_t N_s}\right) - 1 \right] - \frac{V_{PV} + R_s I_{PV}}{R_{sh}} \tag{4}$$

Thereby, N_s stands for the number of series-connected solar cells, α indicates the ideality factor, I_o illustrates the diode saturation current and V_{PV} is the solar panel's output voltage. The following calculation produces the diode's thermal voltage,

$$V_t = \frac{kT}{q} \tag{5}$$

k , q , and T represent the Boltzmann constant, electron charge, and cell temperature, respectively and Table 1 represents the PV parameter specifications.

The PV system's intermittent nature means that the output DC voltage is not high enough to fulfil the load requirement. The adoption of appropriate DC-DC converter topologies improves the low output voltage. The DC/DC converter is designed to control the steady output voltage of the solar cell in a variety of operating scenarios. High gain enhanced Luo converters are used to control and improve the DC voltage to effectively drive the BLDC motor in this study.

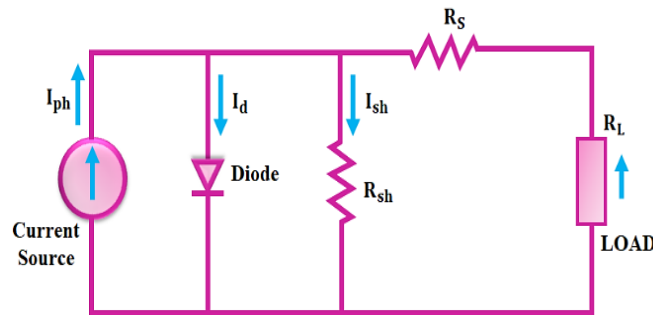


Figure 3. PV cell equivalent circuit

Table 1. PV panel parameter description

Parameters	Values (Units)
Peak power (P_{mp})	100 W
Peak power current (I_{mp})	5.42 A
Peak power voltage (V_{mp})	18.75 V
Number of series connected PV cells N_s	36

3.2. High gain improved Luo converter modelling

The conventional Luo converter has certain drawbacks, such as the need for a large output capacitor to minimize ripple voltage because the output current fluctuates and the inability to function the converters at high duty ratios in order to increase gain. The introduction of a high gain improved Luo converter addresses these shortcomings. Furthermore, this proposed converter offers a high output gain at a low input DC voltage and low duty cycle. The proposed high gain improved Luo converter proceeds in continuous conduction mode with a single switch. The single switch operation decreases the converter's operating stress. The continuous conduction mode (CCM) minimizes the amount of heat generated by power semiconductor devices. Figure 4 shows an improved high gain Boost converter. Single power switches (S), two inductors (L_1, L_2), two input capacitors (C_1, C_2) on output capacitor C_o , and two diodes (D_1, D_2) one output diode D_o comprise this converter.

3.2.1. Modes of operation

There are two distinct states in which converter switches can operate: stage 1 and stage 2.

- Stage 1: ($t_0 - t_1$)

It begins from ($t_0 - t_1$) and the switch S has been activated as seen in Figure 5(a). Therefore, the diodes D_1, D_2 link two capacitors C_1, C_2 and two inductors L_1, L_2 together in parallel to the voltage source V_{in} . The diodes D_1, D_2 are in forward mode throughout this period, while the diode D_o is in reverse state.

- Stage 2: ($t_1 - t_2$)

This state begins at ($t_1 - t_2$) and the switch S has been deactivated as seen in Figure 5(b). The diode D_1, D_2 links the two capacitors C_1, C_2 , the source voltage V_{in} and the two inductors L_1, L_2 in series with the capacitor C_0 loaded by the D_0 . During this time, diode D_0 is in forward mode and diodes D_1, D_2 are in reverse mode.

At the switching (*ON*) period ($t_{on} = DT$)

$$V_{in} = V_{L1} = V_{L2} \quad (6)$$

$$V_{in} = V_{c1} = V_{c2} \quad (7)$$

and at the switching (*OFF*) period ($t_{off} = (1 - D)T$)

$$V_{in} - V_{L1} - V_{L2} + V_{c2} - V_o = 0 \quad (8)$$

as an output, for the obtained switching (*OFF*) period is.

$$V_{L1} = V_{L2} = \frac{3V_{in} - V_o}{2} \quad (9)$$

The derived following results using the voltage-second balance equation between the inductors (L_1 and L_2):

$$V_{in}DT + \frac{3V_{in} - V_o}{2}(1 - D)T = 0 \quad (10)$$

as a result, the voltage transfer ratio from (10) is stated as:

$$\frac{V_o}{V_{in}} = \frac{3 - D}{1 - D} \quad (11)$$

the proposed converter gain voltage (M_D), is.

$$M_D = \frac{V_o}{V_{in}} = \frac{3 - D}{1 - D} \quad (12)$$

Where, M_D is a transfer voltage gain. By the application of high gain improved Luo converter, PV panel output voltage is enhanced. Moreover, conversion efficiency of the suggested converter further improved using efficient hybrid PS-SHO optimized PI controller, which is offers a stabilized DC link output voltage to the 3 ϕ VSI.

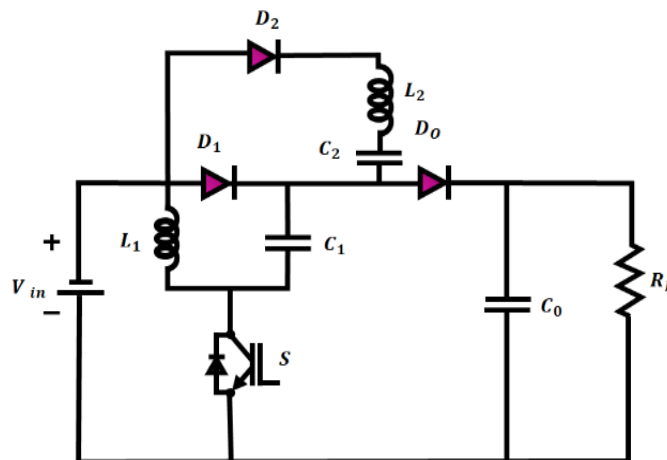


Figure 4. Improved high gain Luo converter

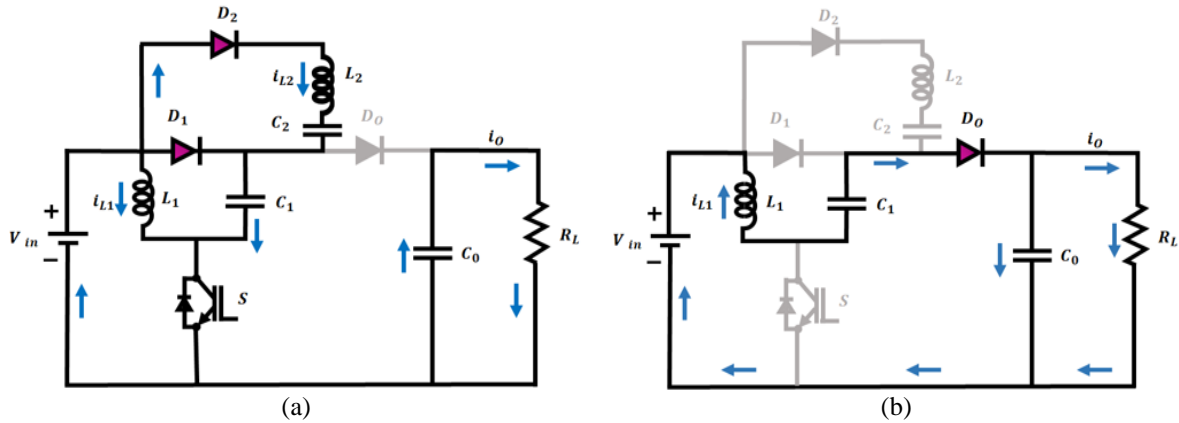


Figure 5. Modes of operation (a) stage 1 ($t_0 - t_1$) and (b) stage 2 ($t_1 - t_2$)

3.3. Hybrid PS-SHO optimized PI controller

3.3.1. PI controller

PI controllers are a type of numerous optimal controllers for a variety of sectors. Utilizing these controllers requires utilizing their modifying elements in order to get the intended outcomes. It is therefore essential to use a method that is both quick and easy to use. These control factors (Kp, Ki) need to be specified. Figure 6 displays the PI controller's operational structure.

A PI-controller is used to control almost every process imaginable, from movement control to aerospace and from slow to fast systems. Certain drawbacks, including a large peak overshoot, susceptibility to controller gains, and a slow response to unexpected disruptions. These limitations are tackled by using the hybrid PS-SHO algorithm, which fine-tunes the parameters of PI controller. In the following section, a detailed explanation of the proposed PS-SHO algorithm is provided.

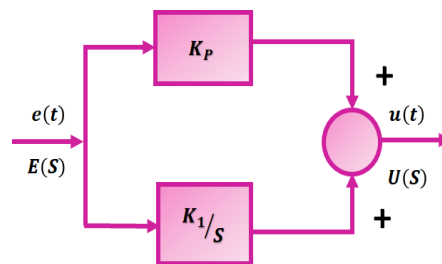


Figure 6. PI Controller

3.3.2. PSO method

PSO is a basic and widely used optimization. A variety of particles have the ability to travel in a multidimensional search space using this approach. During searching, every particle's velocity has to be upgraded.

$$V_i^{k+1} = \omega v_i^k + C_1 rand_1 (P_{i,pbest}^k - x_i^k) + C_2 rand_2 (P_{i,gbest}^k - x_i^k) \tag{13}$$

Here, ω is the starting weight, with values within 0.4 and 0.9 and two independent variables are chosen $rand_1$ and $rand_2$, which fluctuate between $[0, 1]$ and the acceleration coefficients are C_1 and C_2 . The location of the swarm is altered by,

$$x_i^{new} = x_i + v_i \tag{14}$$

Additional iterations lead to a superior response, which is provided by.

$$x_i^{k+1} = \begin{cases} x_{i,new} & \text{iff } f(x_{i,new}) \leq f(x_i) \\ x_i & \text{otherwise} \end{cases} \tag{15}$$

PSO has the main benefit of requiring less variables to be tuned. PSO achieves the most effective solution through particle communication; however, its convergence occurs at an extremely slow pace near the global optimum via a multidimensional search space.

3.3.3. SHO method

The spotted hyena optimizer (SHO) is a bio-inspired metaheuristic optimization method established by Dhiman and Kumar [23]. The method relies on the social behaviors of spotted hyenas, the biggest of three different hyena species (striped, brown, and aardwolf). Spotted hyenas are skilled hunters who hunt in groups, depending on groups with more than 100 members. The SHO algorithm consists of four key processes that mimic the spotted hyena's encircling, hunting, attacking, and searching behaviors of hyenas.

- Prey encircling

The most appropriate solution has been considered as the prospective prey and other search agents adjust their placements in response to the best solution acquired. This behavior's computational framework is presented by (16) and (17):

$$Dh = |B \cdot Pp(x) - P(x)|, \quad (16)$$

$$P(x + 1) = Pp(x) - E \cdot Dh, \quad (17)$$

- Hunting

SHO's hunting approach is outlined as (18) and (19):

$$Pk = Ph - E \cdot Dh, \quad (18)$$

$$Ch = Pk + Pk + 1 \dots + Pk + N, \quad (19)$$

- Attacking prey

The mathematical equation for attacking prey is as (20):

$$P(x + 1) = \frac{ch}{N}, \quad (20)$$

- Searching for prey

Considering the E and B vectors is part of the search for a viable solution. The SHO method is capable of solving a variety of multidimensional issues while avoiding local optimum concerns.

3.3.4. Hybrid PS-SHO algorithm

The PSO method possesses the disadvantage of being confined to local minima when forced to a high restriction, but it has certain benefits such as effectiveness, reliability, and ease of implementation. SHO, on the other hand, avoids becoming imprisoned locally and maintains a balance between exploration and exploitation. As a result, both the outstanding features of PSO and SHO are integrated in the hybrid PS-SHO technique. Figure 7 depicts the flow chart of the hybrid PS-SHO approach and the ensuing sections clarify the way the PS-SHO method is implemented.

Operation of PSO:

- Step 1: Each particles' fitness functions are calculated.
- Step 2: Local *pbest* and global *gbest* values are determined.
- Step 3: All swarm velocity is adjusted utilizing expression (13).
- Step 4: The swarm location has been upgraded utilizing (14).
- Step 5: Every particle's fitness value is evaluated.
- Step 6: Considering (15), the optimum solution for the following iteration is chosen by comparing the fitness value of every particle.

Operation of SHO:

- Step 7: The starting population of SHO is the end population of PSO.
- Step 8: Using the all equations of SHO, the parameters *h*, *B*, *E*, and *N* are updated.
- Step 9: Every search agent is assigned a random position.
- Step 10: The objective function is used to generate fitness values for the spotted hyena.
- Step 11: The location of the spotted hyena and parameters of *Ph* and *Ch* has been updated.
- Step 12: The optimum solution for the next iteration is determined through a comparison of the fitness functions.

- Step 13: By comparing the fitness functions, the optimal solution is chosen for following iteration.
 - Step 14: P_h and C_h are updated.
 - Step 15: The preceding stages are continued until the stop demand is satisfied.
 - Step 16: The final suitable controller parameters have been determined.
- With the implementation of hybrid PS-SHO algorithm, the gain parameter of PI controller is tuned optimally. In addition, the effectiveness of proposed converter enhanced using PS-SHO optimized PI controller.

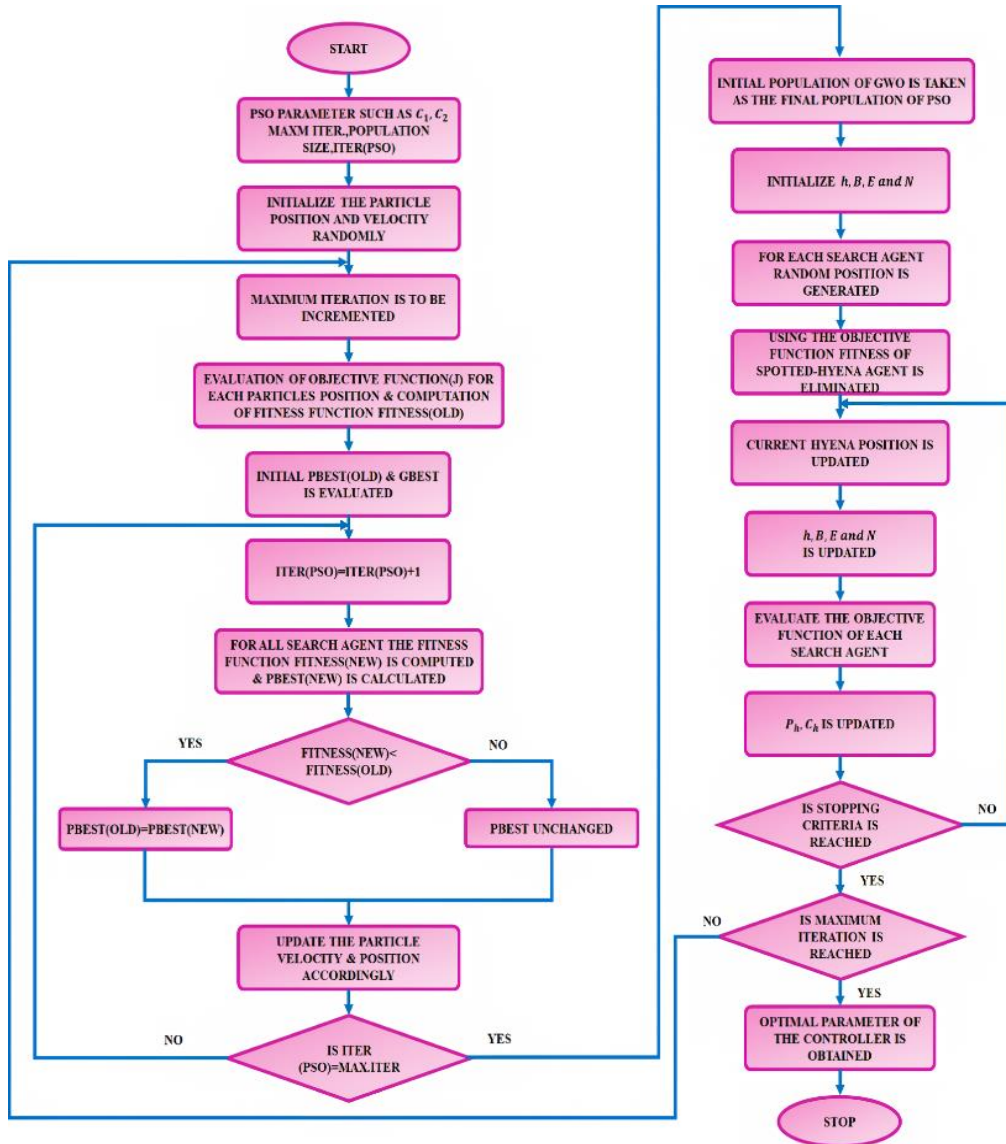


Figure 7. Hybrid PS-SHO flow chart

3.4. BLDC motor modelling

BLDC motors have become prevalent in EVs because of its advantages such as higher dynamic speed and dependability. BLDC motors, compared to ordinary DC motors, lack brushes, leading to minimal servicing and great efficiency. While EVs are powered by BLDC motors, this outperforms induction, DC and switching reluctance motors in terms of technologically superior performance. The BLDC motor is made up of a three stator windings and permanent magnet rotor and, with a trapezoidal flux distribution. The harmonic fields of the stator induce currents in the rotor, however these currents together with stray and iron losses are ignored.

For a system with equilibrium, the mathematical equations of stator windings with respect to of motor electrical characteristics are provided by:

$$V_{an} = R_s i_a + L_{aa} \frac{di_a}{dt} + L_{ab} \frac{di_b}{dt} + L_{ac} \frac{di_c}{dt} + e_a \quad (21)$$

$$V_{bn} = R_s i_b + L_{ba} \frac{di_a}{dt} + L_{bb} \frac{di_b}{dt} + L_{bc} \frac{di_c}{dt} + e_b \quad (22)$$

$$V_{cn} = R_s i_c + L_{ca} \frac{di_a}{dt} + L_{cb} \frac{di_b}{dt} + L_{cc} \frac{di_c}{dt} + e_c \quad (23)$$

The stator resistor per phase R_s is assumed to be identical for all three phases and e_a, e_b, e_c are the induced trapezoidal emf. When there is no variation in the rotor reluctance correlating to the angle generated by non-saliency and three symmetrical phases are considered,

$$L_{aa} = L_{bb} = L_{cc} = L \quad (24)$$

$$L_{ab} = L_{ba} = L_{ac} = L_{ca} = L_{bc} = L_{cb} = M \quad (25)$$

because of the balancing of stator phase currents,

$$i_a + i_b + i_c = 0 \quad (26)$$

thus, the stator winding expressions are can be written as,

$$V_{an} = R_s i_a + (L - M) \frac{di_a}{dt} + e_a \quad (27)$$

$$V_{bn} = R_s i_b + (L - M) \frac{di_b}{dt} + e_b \quad (28)$$

$$V_{cn} = R_s i_c + (L - M) \frac{di_c}{dt} + e_c \quad (29)$$

and the obtained electromagnetic torque is:

$$T_e = \frac{e_a i_a + e_b i_b + e_c i_c}{\omega_m} \quad (30)$$

where T_e the electromagnetic torque and ω_m is the angular speed in radians per second. By comparing the reference speed N_{ref} with the actual speed N_{act} , the PI controller controls the speed of the 3 ϕ BLDC motors, as seen in Figure 8.

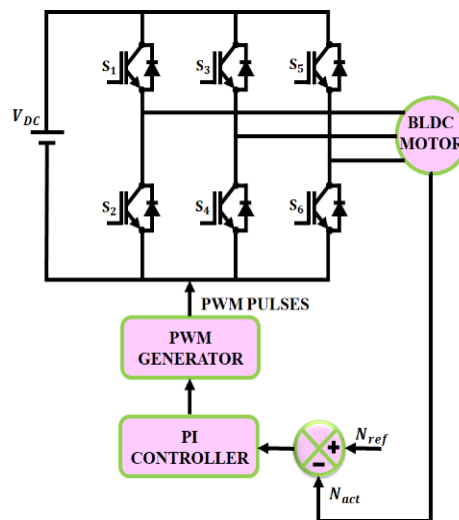


Figure 8. Regulation of BLDC motor using PI controller

4. RESULTS AND DISCUSSION

This research focuses on a PV-based BLDC motor with a PI controller and a hall sensor for continuous speed regulation. Increasing the PV output with lesser ripples and power loss through the use of a high gain improved Luo converter. A hybrid PS-SHO optimized PI controller is deployed to increase the switching efficacy of recommended converter. To construct a grid-interactive system that supplies electricity at night while accepting excess solar power during the day. This graph shows the overall performance of the recommended system when tested using the MATLAB platform. Table 2 shows the parameter design of the proposed system.

Table 2. Parameter description

	Parameters	Values
PV Panel	Open circuit voltage V_{OC}	22.68 V
	Short circuit current I_{SC}	5.86 A
	Peak power	100 W, 15 Panels
	Number of series connected PV cells N_s	36
High Gain Improved Luo Converter	Switching Frequency	10 KHz
	L_1, L_2, L_3	0.288 mH
	C_1, C_2	4.6 μ F
	C_o	220 μ F
BLDC motor	Speed	3000 rpm
	Load inertia (J)	9×10^{-4} Nm ²

As illustrated in Figure 9(a), a temperature variation of 0.25 s is created to assess the efficacy of the recommended technique to tackle the intermittent behavior of the PV system. At the same time, the temperature increases abruptly from 25 °C to 35 °C. Figure 9(b) depicts the irradiation of a PV system ranging from 800 W/Sq.m to 1000 W/Sq.m.

The output current and voltage of PV panel is indicated in Figure 10. The temperature variation at 0.25 s, which affects the PV panel's current and voltage. According to the waveform Figures 10(a) and 10(b), the voltage rises from 50 V to 60 V, the current reaches a peak value of 40 A and after 0.26 s and it becomes stable with small distortions respectively. The recommended high gain Improved Luo converter boosts the produced PV voltage.

The high gain Improved Luo converter simulation result is highlighted in Figure 11, which shows that the PS-SH optimized PI controller is successful in maintaining a constant dc-link voltage of 330 V while reducing settling time by 0.1 s as seen in Figures 11(a) and 11(b) correspondingly. The proposed improved controller settles more quickly than the standard PI controller. Similar to that, the Figure 11(c) illustrates the steady current 0.2 A is kept preserved after 0.3 seconds. The waveforms for grid voltage and current are illustrated in Figure 12, which demonstrates that 230 V and 9 A are maintained correspondingly as seen in Figures 12(a) and 12(b). As shown in Figure 13, the actual power of 200 W is attained after 0.28 seconds and the current is maintained after 0.06 seconds, which are illustrated in Figures 13(a) and 13(b) accordingly.

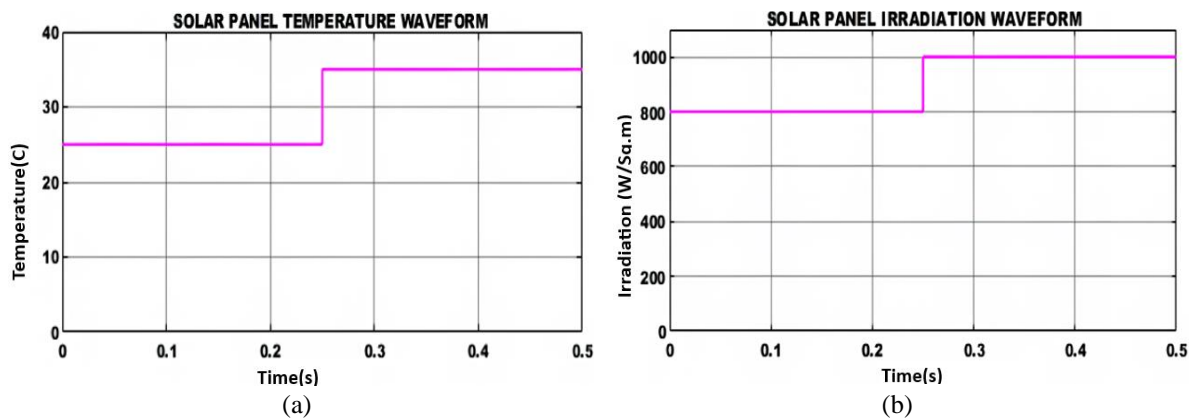


Figure 9. Waveforms demonstrating PV panel (a) temperature and (b) irradiation

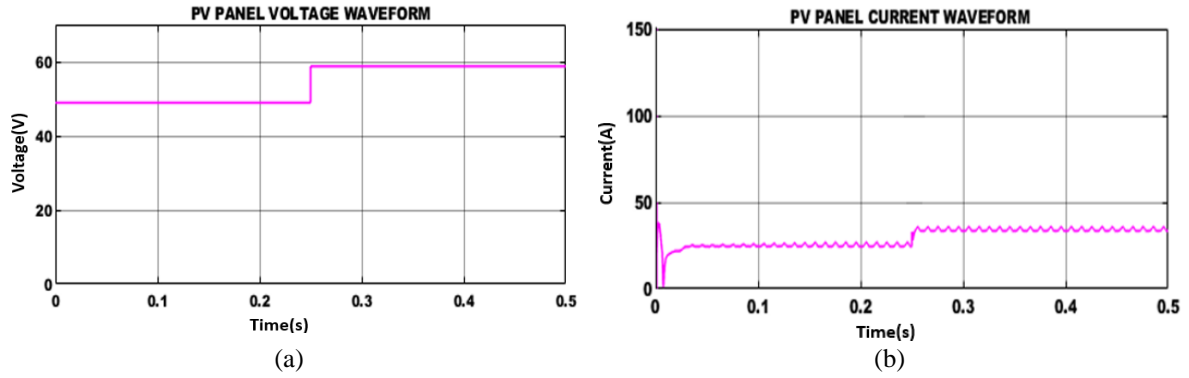


Figure 10. Waveforms demonstrating PV panel (a) voltage and (b) current

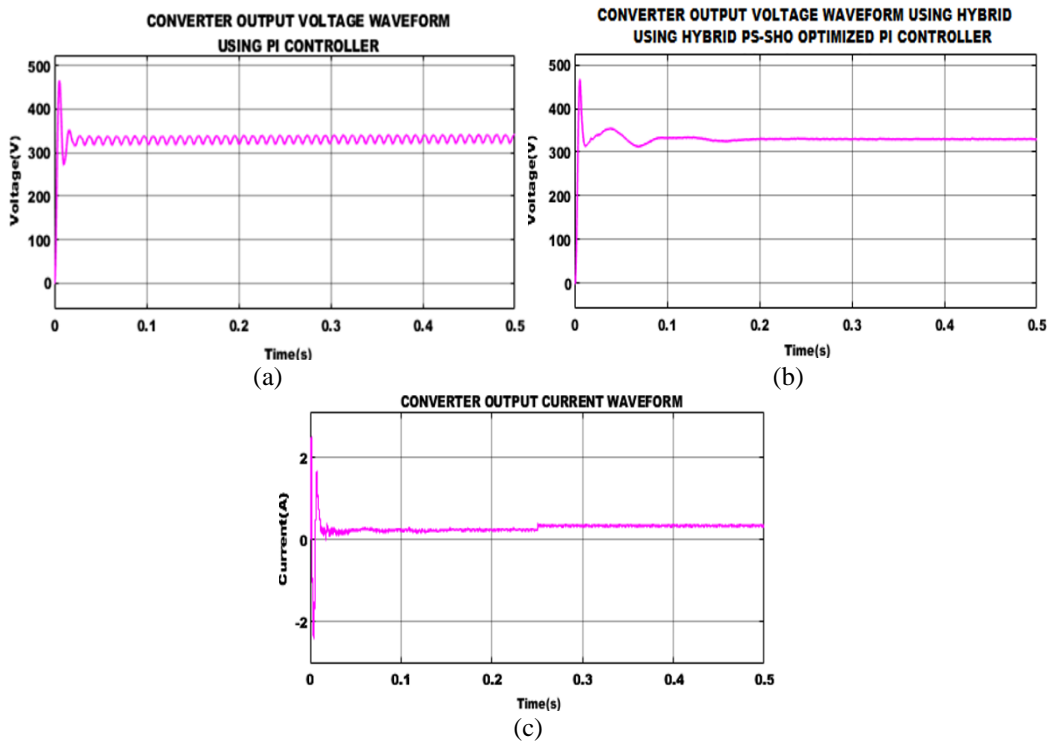


Figure 11. Waveforms demonstrating output of converter voltage using (a) PI controller, (b) PS-SHO optimized PI controller, and (c) output current

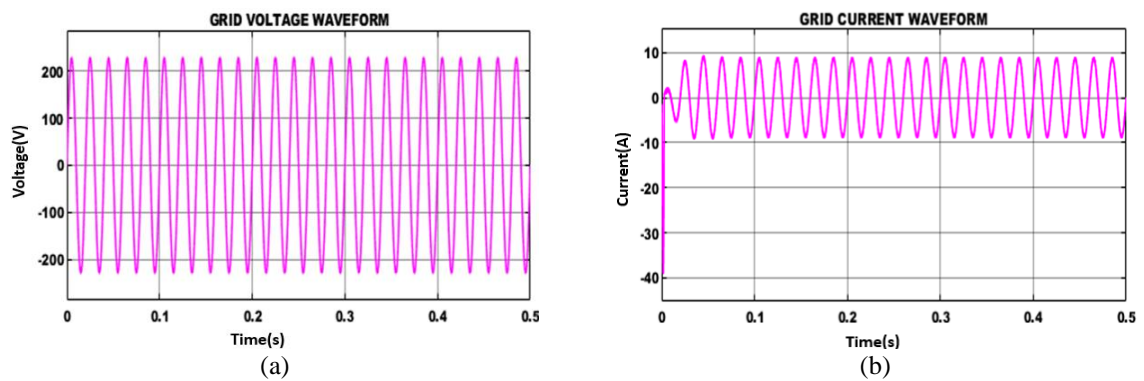


Figure 12. Output waveforms of grid side (a) voltage and (b) current

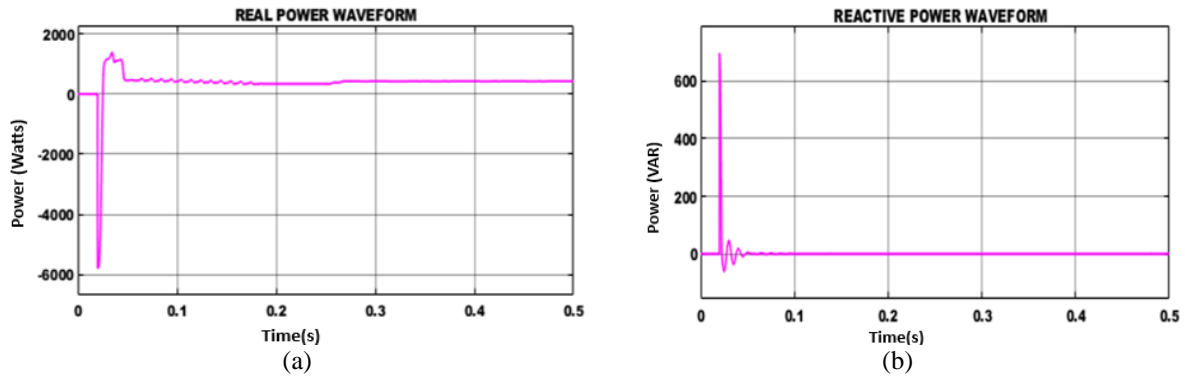


Figure 13. Output waveforms of grid side (a) real power and (b) reactive power

When a mechanical load is applied to the motor shaft, opposing forces are created that the motor must overcome. The motor must produce additional torque to offset the load torque in order to keep rotating or increase speed. Depending on the load, this causes an increase in motor current and torque output to maintain or vary the speed. The change in torque in a BLDC motor is a natural response to changes in load and speed. To overcome external resistance and maintain the desired speed, the motor adjusts its torque output. Here, the BLDC motor's current, speed, back electromagnetic force (EMF) and torque are illustrated in Figure 14. The increased torque and starting current of the BLDC motor allow it to start up at a low speed. The motor's speed doesn't change as the current amplitude does. The motor's current consumption throughout operation is quite small. For smooth and consistent operation, a maximum speed of roughly 2000 rpm is shortly reached. As seen in Figure 15, the proposed strategy minimizes THD to 2.02%.

Table 3 represents the efficiency analysis of proposed converter in contrasted to another converter, the corresponding plot represented in Figure 16. The graph makes it abundantly evident that the suggested high gain enhanced Luo converter has the highest efficiency of 97.3% and the lowest ripple contents. Similarly, the comparison of THD is indicated in Figure 17, from the observation is it noted that the suggested system has reduced THD value in contrasted to other approaches. The PI controller with optimized PI controller comparison is indicated in Table 4. Here, the proposed hybrid PS-SHO optimized PI controller accomplishes very quick settling time of 0.23 s while compared to classical PI, GA tuned PI, PSO tuned PI, GWO tuned PI, and SHO tuned PI controllers.

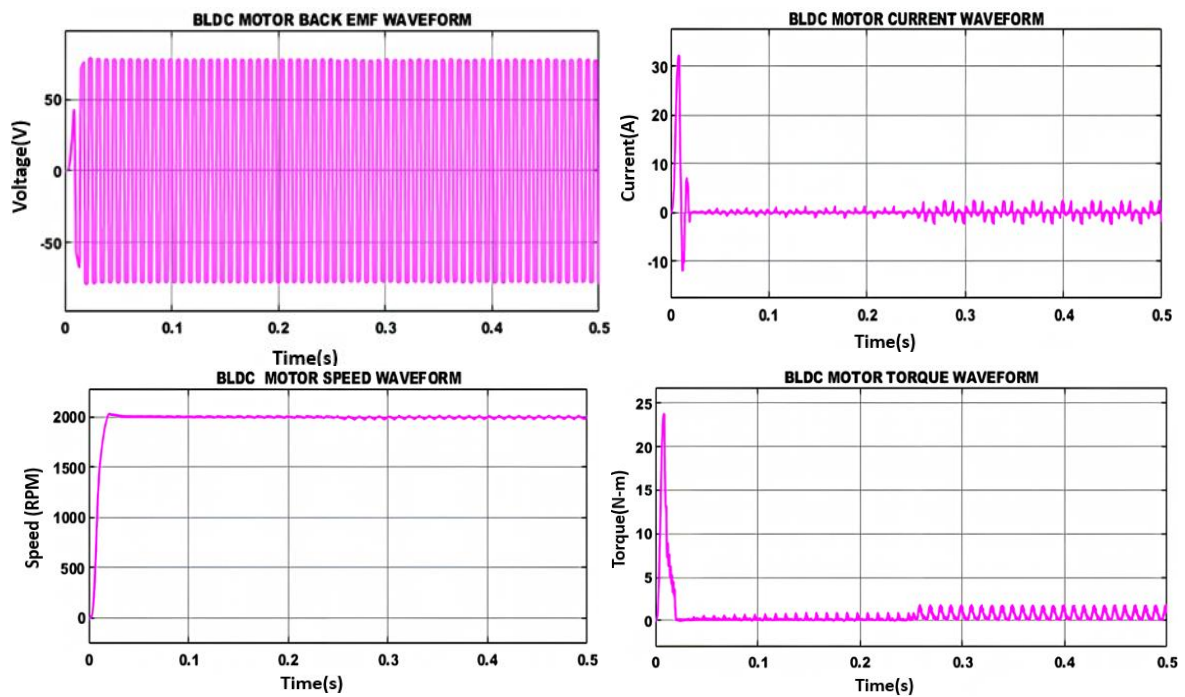


Figure 14. Waveforms for BLDC motor parameters

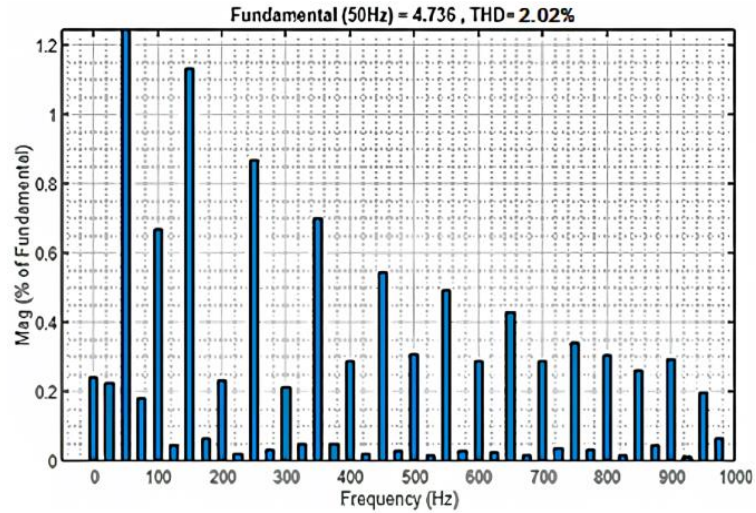


Figure 15. THD

Table 3. Comparison analysis of converter

Converter	Efficiency%
Interleaved DC-DC [24]	94.85%
Single Phase LLC [25]	95.8%
DAB [26]	96.7%
Transformer less converter [27]	95.2%
Proposed converter	97.3%

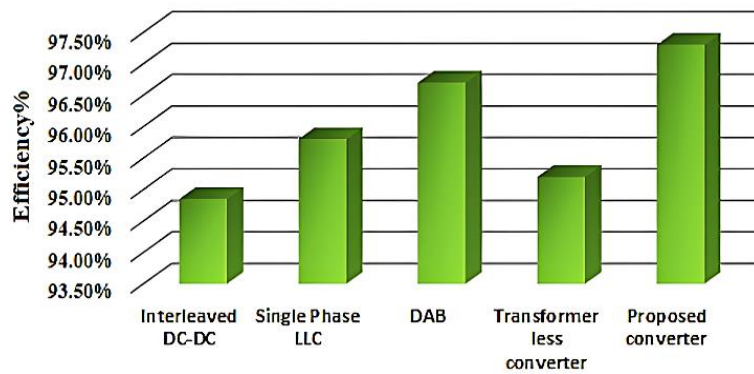


Figure 16. Comparison analysis of efficiency

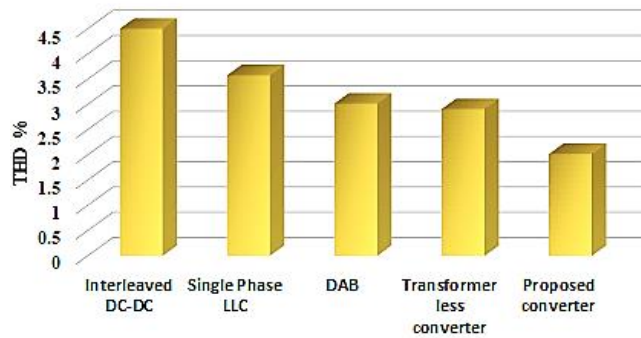


Figure 17. Comparison analysis of THD

Table 4. Comparison analysis of controller

Controller	Parameter		
	Rise time (t_r)	Peak time (t_p)	Settling time (t_s)
PI	0.01 s	0.01 s	-
GA-PI	0.09s	0.05s	0.52s
PSO-PI	0.1 s	0.09 s	0.43 s
GWO-PI	0.07 s	0.08s	0.39s
SHO-PI	0.08 s	0.07s	0.32 s
Hybrid PS-SHO-PI	0.01 s	0.01 s	0.23 s

5. CONCLUSION

This paper proposes a grid-integrated PV supplied EV based BLDC motor with a DC-to-DC converter and a hybrid optimized PI controller. A novel high gain Luo converter has been developed to address the oscillating properties of PV systems and it provides the outstanding advantages of a high conversion range, low voltage stress and exceptional performance. The recommended converter's efficiency is greatly increased by the trustworthy hybrid PS-SHO optimized PI controller. A PI controller then controls the motor speed. The BLDC motor uses grid's supply of electricity in the event that the PV based power source fails. The MATLAB simulation used to assess the suggested EV motor's efficient functioning verifies the approach's increased efficacy, with an optimum efficiency of 97.3% and a reduced THD of 2.02%.





REFERENCES

- [1] K. S. Kavim and P. S. Karavelam, "PV-based grid interactive PMBLDC electric vehicle with high gain interleaved DC-DC SEPIC Converter," *IETE Journal of Research*, vol. 69, no. 7, pp. 4791–4805, Sep. 2023, doi: 10.1080/03772063.2021.1958070.
- [2] J. A. Glenn and S. Alavandar, "Hybrid optimized PI controller design for grid tied PV based electric vehicle," *Intelligent Automation & Soft Computing*, vol. 36, no. 2, pp. 1523–1545, 2023, doi: 10.32604/iasc.2023.033545.
- [3] B. Saha and B. Singh, "SMO based position sensorless BLDC motor drive employing canonical switching cell converter for light electric vehicle," in *2021 IEEE International Power and Renewable Energy Conference (IPRECON)*, IEEE, Sep. 2021, pp. 1–6, doi: 10.1109/IPRECON52453.2021.9640796.
- [4] A. D. G. Jegha, M. S. P. Subathra, N. Manoj Kumar, U. Subramaniam, and S. Padmanaban, "A high gain DC-DC converter with grey wolf optimizer based MPPT algorithm for PV fed BLDC motor drive," *Applied Sciences*, vol. 10, no. 8, p. 2797, Apr. 2020, doi: 10.3390/app10082797.
- [5] S. Mishra, A. Varshney, B. Singh, and H. Parveen, "Driving-cycle-based modeling and control of solar-battery-fed reluctance synchronous motor drive for light electric vehicle with energy regeneration," *IEEE Transactions on Industry Applications*, vol. 58, no. 5, pp. 6666–6675, Sep. 2022, doi: 10.1109/TIA.2022.3181224.
- [6] A. K. Mishra, A. K. Singh, and G. M. Vishwanath, "A fuel-efficient BLDC motor-driven light electric vehicle with single-stage onboard charging system," *IEEE Transactions on Transportation Electrification*, vol. 9, no. 4, pp. 4909–4921, Dec. 2023, doi: 10.1109/TTE.2022.3226536.
- [7] R. Kumar and B. Singh, "Solar PV powered-sensorless BLDC motor driven water pump," *IET Renewable Power Generation*, vol. 13, no. 3, pp. 389–398, Feb. 2019, doi: 10.1049/iet-rpg.2018.5717.
- [8] G. G. R. Sekhar and B. Banakara, "An internal current controlled BLDC motor drive supplied with PV fed high voltage gain DC-DC converter," *International Journal of Electrical and Computer Engineering (IJECE)*, vol. 8, no. 2, p. 1262, Apr. 2018, doi: 10.11591/ijece.v8i2.pp1262-1272.
- [9] A. K. Singh, M. Badoni, and Y. N. Tatte, "A multifunctional solar PV and grid based on-board converter for electric vehicles," *IEEE Transactions on Vehicular Technology*, vol. 69, no. 4, pp. 3717–3727, Apr. 2020, doi: 10.1109/TVT.2020.2971971.
- [10] D. S. Nayak and R. Shivarudraswamy, "Solar fed BLDC motor drive for mixer grinder using a boost converter," *International Journal of Power Electronics and Drive Systems (IJPEDS)*, vol. 11, no. 1, p. 56, Mar. 2020, doi: 10.11591/ijpeds.v11.i1.pp56-63.
- [11] S. Chandra, P. Gaur, and D. Pathak, "Radial basis function neural network based maximum power point tracking for photovoltaic brushless DC motor connected water pumping system," *Computers & Electrical Engineering*, vol. 86, p. 106730, Sep. 2020, doi: 10.1016/j.compeleceng.2020.106730.
- [12] G. G. R. Sekhar and B. Banakar, "Solar PV fed non-isolated DC-DC converter for BLDC motor drive with speed control," *Indonesian Journal of Electrical Engineering and Computer Science*, vol. 13, no. 1, p. 313, Jan. 2019, doi: 10.11591/ijeecs.v13.i1.pp313-323.
- [13] Z. Karami, Q. Shafiee, S. Sahoo, M. Yaribeygi, H. Bevrani, and T. Dragicevic, "Hybrid model predictive control of DC-DC Boost converters with constant power load," *IEEE Transactions on Energy Conversion*, vol. 36, no. 2, pp. 1347–1356, Jun. 2021, doi: 10.1109/TEC.2020.3047754.
- [14] P. Azer and A. Emadi, "Generalized state space average model for multi-phase interleaved Buck, Boost and Buck-Boost DC-DC Converters: transient, steady-state and switching dynamics," *IEEE Access*, vol. 8, pp. 77735–77745, 2020, doi: 10.1109/ACCESS.2020.2987277.
- [15] R. Kumar and B. Singh, "Solar PV powered BLDC motor drive for water pumping using Cuk converter," *IET Electric Power Applications*, vol. 11, no. 2, pp. 222–232, Feb. 2017, doi: 10.1049/iet-epa.2016.0328.
- [16] S. K. Jahan, K. Chandru, B. Dhanapriyan, R. K. Kumar, and G. Vinothraj, "SEPIC converter based water driven pumping system by using BLDC motor," *Bonfring International Journal of Power Systems and Integrated Circuits*, vol. 7, no. 1, pp. 07–12, Mar. 2017, doi: 10.9756/BIJPSIC.8317.
- [17] R. Femi, T. S. R. Raja, and R. Shenbagalakshmi, "A positive output-super lift Luo converter fed brushless DC motor drive using alternative energy sources," *International Transactions on Electrical Energy Systems*, vol. 31, no. 2, Feb. 2021, doi: 10.1002/2050-7038.12740.
- [18] Y. Li *et al.*, "Electrochemical Model-based fast charging: physical constraint-triggered PI control," *IEEE Transactions on Energy Conversion*, vol. 36, no. 4, pp. 3208–3220, Dec. 2021, doi: 10.1109/TEC.2021.3065983.





- [19] M. A. Ibrahim, A. K. Mahmood, and N. S. Sultan, "Optimal PID controller of a brushless dc motor using genetic algorithm," *International Journal of Power Electronics and Drive Systems (IJPEDS)*, vol. 10, no. 2, p. 822, Jun. 2019, doi: 10.11591/ijpeds.v10.i2.pp822-830.
- [20] V. Kumarasamy, V. K. Ramasamy, and G. Chinnaraj, "Systematic design of multi-objective enhanced genetic algorithm optimized fractional order PID controller for sensorless brushless DC motor drive," *Circuit World*, vol. 48, no. 4, pp. 479–492, Nov. 2022, doi: 10.1108/CW-07-2020-0137.
- [21] P. Srivastava and V. K. Tiwari, "Speed control of BLDC motor fed from solar PV Array using particle swarm optimization," in *2020 9th International Conference System Modeling and Advancement in Research Trends (SMART)*, IEEE, Dec. 2020, pp. 392–397, doi: 10.1109/SMART50582.2020.9337111.
- [22] R. Sreedhar, P. Chandrasekar, K. Karunanithi, S. C. Vijayakumar, and S. P. Raja, "Design and validation of a single-phase Buck–Boost inverter with Grey Wolf optimization algorithm under partial shaded conditions," *International Journal of Information Technology*, vol. 14, no. 7, pp. 3667–3677, Dec. 2022, doi: 10.1007/s41870-022-00948-3.
- [23] G. Dhiman and V. Kumar, "Multi-objective spotted hyena optimizer: A Multi-objective optimization algorithm for engineering problems," *Knowledge-Based Systems*, vol. 150, pp. 175–197, Jun. 2018, doi: 10.1016/j.knosys.2018.03.011.
- [24] H. Ye, G. Jin, W. Fei, and N. Ghadimi, "High step-up interleaved DC/DC converter with high efficiency," *Energy Sources, Part A: Recovery, Utilization, and Environmental Effects*, pp. 1–20, Jan. 2020, doi: 10.1080/15567036.2020.1716111.
- [25] X. Zhou *et al.*, "A High-Efficiency High-power-density on-board low-voltage DC–DC converter for electric vehicles application," *IEEE Transactions on Power Electronics*, vol. 36, no. 11, pp. 12781–12794, Nov. 2021, doi: 10.1109/TPEL.2021.3076773.
- [26] T.-R. Granados-Luna *et al.*, "Two-phase, dual interleaved Buck–Boost DC–DC converter for automotive applications," *IEEE Transactions on Industry Applications*, vol. 56, no. 1, pp. 390–402, Jan. 2020, doi: 10.1109/TIA.2019.2942026.
- [27] N. D. Dao, D.-C. Lee, and Q. D. Phan, "High-efficiency sic-based isolated three-port DC/DC converters for hybrid charging stations," *IEEE Transactions on Power Electronics*, vol. 35, no. 10, pp. 10455–10465, Oct. 2020, doi: 10.1109/TPEL.2020.2975124.

BIOGRAPHIES OF AUTHORS



S. Prakash     serving as an academicians for more than a decade and currently working as Assistant Professor (G-II) in the Department of Electrical and Electronics Engineering at Aarupadai Veedu Institute of Technology, Vinayaka Mission's Research Foundation (Deemed to be University) Chennai. He received his B.E. in Electrical and Electronics Engineering from Government college of Engineering and M.E in Power system Engineering from Annamalai University. He has more than 15 publications in the field of Power system engineering, special machines, and renewable energy technology. Currently Pursuing his Ph.D. degree at Vinayaka Mission's Research Foundation (Deemed to be University). He can be contacted at email: prakash.yours@gmail.com.



K. Boopathy     received the B.E. from Madras University (Electrical and Electronics Engineering) in 1999, M.E. in Electronic Engineering from Anna University (MIT campus) in 2003, and Ph.D. in Power Electronics from Anna University, Chennai in 2012. Currently he is working as Professor in Department. of Electrical and Electronics Engineering Aarupadai Veedu Institution of technology, VMRF Chennai. He has published several National and International Journals and Conferences. His area of interest is power electronics and drives, soft computing technique application to power electronics, and electrical machines. He can be contacted at email: boopathyk@avit.ac.in.